

Enhancing Virtual Try-On with Synthetic Pairs and Error-Aware Noise Scheduling

Nannan Li
Boston University
nnli@bu.edu

Kevin J. Shih
NVIDIA

Bryan A. Plummer
Boston University
bplum@bu.edu

Abstract

Given an isolated garment image in a canonical product view and a separate image of a person, the virtual try-on task aims to generate a new image of the person wearing the target garment. Prior virtual try-on works face two major challenges in achieving this goal: a) the paired (human, garment) training data has limited availability; b) generating textures on the human that perfectly match that of the prompted garment is difficult, often resulting in distorted text and faded textures. Our work explores ways to tackle these issues through both synthetic data as well as model refinement. We introduce a garment extraction model that generates (human, synthetic garment) pairs from a single image of a clothed individual. The synthetic pairs can then be used to augment the training of virtual try-on. We also propose an Error-Aware Refinement-based Schrödinger Bridge (EARSB) that surgically targets localized generation errors for correcting the output of a base virtual try-on model. To identify likely errors, we propose a weakly-supervised error classifier that localizes regions for refinement, subsequently augmenting the Schrödinger Bridge’s noise schedule with its confidence heatmap. Experiments on VITON-HD and DressCode-Upper demonstrate that our synthetic data augmentation enhances the performance of prior work, while EARSB improves the overall image quality. In user studies, our model is preferred by the users in an average of 59% of cases.

1. Introduction

Virtual try-on aims to generate a photorealistic image of a target person wearing a prompted product-view garment [23, 37, 40]. It allows users to visualize how garments would fit and appear on their bodies without the need for physical trials. While recent methods have made significant strides in this field [19, 30, 36, 37], noticeable artifacts such as text distortion and faded textures persist in gener-



Figure 1. Example of our proposed Error-Aware Refinement Schrödinger Bridge (EARSB). EARSB can refine the artifacts (marked by bounding boxes) in an initial image generated by an existing try-on model. The initial image is generated by [19] in the top row and by [30] in the bottom row. + Syn. Data in the last column strengthens the refinement with the proposed synthetic data augmentation in training.

ated images. For example, as illustrated in the second row of Fig. 1, the logo and the text on the t-shirt noticeably fade away in the initial image generated by a prior try-on model [30]. These imperfections stem from two primary challenges in virtual try-on: limited data availability and the complexity of accurate garment texture deformation. Addressing the issues, we propose a two-pronged approach: augmenting training data through cost-effective synthetic data generation, and surgically targeting known generation artifacts using our proposed Error-Aware Refinement-based Schrödinger Bridge (EARSB).

At a minimum, the training data of virtual try-on requires paired (human, product-view garment) images. The product-view garment image is a canonical, front-facing view of the clothing with a clean background. A substantial amount of data is needed to capture the combinatorial space

comprising all possible human poses, skin tones, viewing angles, and their respective physical interactions with fabric textures, shapes, letterings, and other material properties. Unfortunately, these images are generally available only on copyright-protected product webpages and therefore not readily available for use. To mitigate this issue, we propose to augment training with synthetic data generated from the easier symmetric human-to-garment task, wherein we train a garment-extraction model to extract a canonical product-view garment image from an image of a clothed person. This will allow us to create synthetic *paired* training data from unpaired datasets [12, 25, 35]. Our results demonstrate that incorporating the more readily available synthetic training pairs can improve image generation quality in the virtual try-on task.

In addition to addressing the data scarcity issue, we aim to construct a refinement model that can make localized adjustments to a weaker model’s generation results. Our approach draws inspiration from classical boosting approaches where every model in a cascade of models targets the shortcomings of the preceding models. We are interested in a targeted refinement approach for two main reasons: it allows a training objective that is focused solely on fixing specific errors, and potentially saves computation when initial predictions are sufficiently good.

Two components are necessary to achieve such a pipeline: a classifier for identifying localized generation errors, and a refinement model that can re-synthesize content specifically in these localized regions. We found that an effective Weakly-Supervised Classifier (WSC) can be constructed with just a few hours of manual labeling of generation errors. Another benefit of this approach is that it can be easily tailored for the errors of a specific model that produces images with artifacts. The resulting WSC will produce an error map highlighting low-quality regions. Subsequently, we adopt an Image-to-Image Schrödinger Bridge (I^2SB) [24] to learn the refinement of these regions in the generated images. While typical diffusion models map from noise to data, I^2SB constructs a Schrödinger Bridge (SB) that allows us to map from data to data, or in our setup, generations with artifacts to ground truth images. In addition, we introduce an *adaptive* noise schedule to direct the SB process to focus on the localized errors by incorporating the classifier’s prediction error into the noise schedule, which we describe in more detail in Sec. 5.1. In the first row of Fig. 1, our refinement SB model (*i.e.*, EARSB) corrects the distorted text in the initially generated image.

The contributions of our paper are:

- We introduce (human, synthetic garment) pairs as an augmentation in the training of virtual try-on task. The synthetic garment is obtained from our human-to-garment model, which can generate product-view garment images from human images.
- We introduce a spatially adaptive Schrödinger Bridge model (EARSB) to refine the outputs of a base virtual try-on model. Our formulation incorporates a *spatially varying* diffusion noise schedule, with noise proportional to the degree of refinement we wish to perform locally. We find this to yield better results than the baseline Schrödinger Bridge framework.
- Extensive experiments on two datasets (VITON-HD [21] and DressCode-Upper [26]) show that EARSB enhances the quality of the images generated by prior work, and is preferred by the users in 59% cases on average.

2. Related Work

Training with Synthetic Data. The addition of synthetic data is often an effective means of improving downstream task performance when it is difficult to amass real data at the necessary scale. This has been demonstrated in the domains of image generation [18, 31] and image editing [5, 34]. Careful applications can also be used to ameliorate dataset imbalance issues, as shown in [10]. Other works such as [1] use self-synthesized data to provide negative guidance for the diffusion model. Our incorporation of synthetic data in the virtual try-on task tackles a specific sub-problem in the broader image editing domain and is similar in spirit to [5, 34]. Specifically, we aim to synthesize paired training data that satisfies the stringent requirements of virtual try-on paired training data – a canonical product-view garment image paired with an example of it being worn. Images of people in clothing are readily available, but it is difficult to obtain a product-view image of the exact clothing they are wearing. To address this, our work proposes and tackles the human-to-garment, which is roughly symmetric to the virtual try-on task and aims to extract the clothing from a person’s photo and project it to the canonical product view.

Virtual Try-On. There has been a shift from earlier GAN-based framework [15, 21, 23, 30, 36] to diffusion-based methods [7, 19] in the virtual try-on literature. Diffusion models fit an SDE process mapping from the image distribution to the noise distribution, and tend to be easier to train than GAN-based approaches due to the simplicity of the L2 denoising loss [11, 13, 32]. At inference, the diffusion model denoises a random Gaussian noise distribution to a human-readable image via multiple sampling steps. [7, 37] propose parameter-efficient approaches that concatenate the human image and the garment images along the spatial dimension such that the self-attention layer in the denoising UNet can achieve texture transfer without extra parameters. In [19], the authors introduce additional cross-attention layers to learn the semantic correspondences between the garment and the human image. The methods in [3, 22, 28] align different embedding spaces in the attention module to achieve flexible clothing editing after try-on, such as style change or graphics insertion. In contrast to



Figure 2. (a) Our human-to-garment model, which is explained in Sec. 4.1 (b) Examples of the constructed (human, synthetic garment) pairs in Sec. 4.1.

prior work that samples from random noise, we build upon recent advances in Schrödinger bridges, notably [24], to directly sample from an initial image generated by prior try-on models. Our work is similar in spirit to [38], which initializes the noisy image with a GAN-generated image and small amounts of random noise. However, our work explores varying the local noise schedule based on the error level at a given location.

3. Virtual Try-On Task Definition

Let (x_0, C) be the (human image, product-view of worn garment) pair in virtual try-on training. We will refer to (x_0, C) as paired data. Let \bar{x}_0 be a masked version of x_0 in which the worn garment corresponding to C is masked out. We can then set up a learning task in which we aim to fit the following function: $F(\bar{x}_0, C, \phi; \theta) \rightarrow x_0$, where ϕ corresponds to other conditionals such as pose representations from DensePose [14].

4. Augmented Training with Synthetic Data

Acquiring high-quality pairs (x_0, C) at scale is challenging due to copyright and brand protection. On the other hand, acquiring images of just humans (x_0) at scale is considerably more feasible [12, 22, 25, 35]. This observation motivates our proposal of the human-to-garment task to extract a synthetic canonical view image \hat{C} from x_0 . We can

then augment our virtual try-on training with (x_0, \hat{C}) pair, requiring only single human images. In the following, we explain the architecture of our human-to-garment model in Sec. 4.1, how we use it to construct the synthetic dataset in Sec. 4.2, and how the synthetic data is used to augment the virtual try-on training in Sec. 4.3.

4.1. Human-to-Garment Model

While virtual try-on requires generating skin and deforming the product-view garment to accommodate diverse postures, the human-to-garment task simply aims to map the clothing item to its canonical view. To achieve this, we use existing paired (human, garment) data (e.g., VITON-HD [21]) to train our human-to-garment model. As illustrated in Fig. 2a, we first segment and extract the clothing on the person map and then feed the clothing item to a generator that synthesizes its canonical view. The generator is based on the UNet model proposed in [15], which uses a flow-like mechanism for warping latent features in an optical-flow-like manner. The generator was trained using a combined L1 reconstruction and adversarial loss.

4.2. Constructing Synthetic H2G-UH and H2G-FH

Synthetic images \hat{C} produced from our models necessarily contain generation errors. We use the following criteria to filter for high-quality synthetic data: a) The single human image x_0 has a clean background (low pixel variance in the non-human region); b) x_0 is frontal view (classified by its DensePose representation [14]); c) the reconstruction error (LPIPS distance) is small when reconstructing the human image x_0 in a try-on model using the (x_0, \hat{C}) pair (e.g., [21, 30]). Under these criteria, we select human images from DeepFashion2 [25] and UPT [35], eventually creating 12,730 synthetic pairs of upper-body human images (referred to as H2G-UH) and 8,939 pairs of full-body human images (referred to as H2G-FH). Examples of the synthetic pairs are shown in Fig. 2b.

4.3. Augmented Virtual Try-on Training

To further prevent distribution leakage of incorporating synthetic data, we explore two means of limiting the effect of the real-synthetic domain gap: (a) two training stages involving pretraining the try-on model using synthetic pairs, and then finetuning on real pairs [20]; (b) training simultaneously on real and synthetic data, but conditioning the try-on model on a real/synthetic flag, similarly to [17]. We found empirically that the second augmentation performs slightly better than the first (See Sec. 6.1).

5. Error-Aware Refinement Schrödinger Bridge

Apart from the synthetic data augmentation, our second approach to enhancing existing try-on methods is a refine-

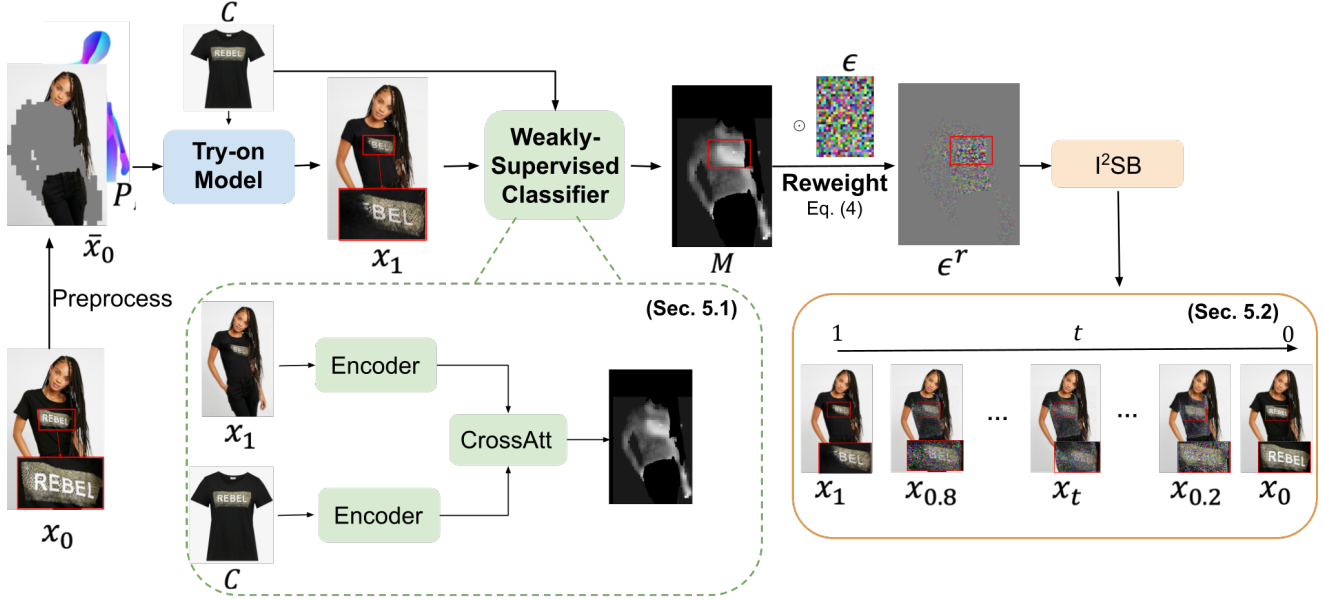


Figure 3. The diffusion process in our refinement-based EARSB. We first preprocess the input image, then use a base try-on model that takes the masked human image \bar{x}_0 , its pose representation P , and its garment C as input to generate an initial human image x_1 . x_1 is fed to our weakly-supervised classifier (WSC) to obtain the error map M (see Sec. 5.1). This map reweights the noise distribution ϵ to ϵ^r in I^2SB diffusion and refines x_1 that has generation errors to the ground truth image x_0 (see Sec. 5.2).

ment pipeline in two steps: identifying the errors in the generated try-on image, referred to as x_1 , and then fitting a targeted model that learns to refine the erroneous locations in x_1 . Given some base model $F_{base}(\bar{x}_0, C, \phi) \rightarrow x_1$ where $F_{base}(\cdot)$ can be any pretrained GAN or diffusion-based approach to virtual try-on, x_1 closely approximates the true real human image x_0 with some generation artifacts. To automatically identify the artifacts in x_1 , we construct a weakly-supervised error classifier $WSC(x_1, C) \rightarrow M$ as in Fig. 3, where M is a confidence map predicting a heatmap for likely generation errors. Then, we perform the final refinement by fitting a Schrödinger bridge based on I^2SB [24] that can perform the following mapping: $F_{EARSB}(x_1, C, M, \phi; \theta) \rightarrow x_0$.

The approach is weakly inspired by boosting methods in that we wish to fit a *targeted* refinement model that is trained specifically on the generation errors of an existing model. The refinement goal applies to the general setting where we want to refine a flawed image output, though we focus on virtual try-on for this work.

As in Fig. 3, the training of EARSB includes three steps:

1. Pre-process the images in the training set and feed them to existing try-on models to get the initial images x_1 .
2. Obtain the error maps M on the initial images x_1 using our WSC (Sec. 5.1).
3. Use M to adjust the noise schedule in I^2SB [24] and train the noise prediction model in EARSB following Eq. 9 (Sec. 5.2).

In the following, we start with explaining step 2 as step 1 is simply running prior try-on models.

5.1. Obtaining the Error Map

We start by obtaining the error map M that highlights the corrupted or incorrect area of the initial image x_1 . A weakly-supervised classifier (WSC) is introduced to predict this error map.

Classifier Architecture. As shown in the green dotted box of Fig. 3, our WSC has two encoders to match the image features of x_1 and C with cross attention to predict a sigmoid-activated error map.

Training Data Annotation. In practice, it is labor-intensive to fully annotate all the initial images for where the generated artifacts are located. To mitigate this issue, we used a few hours to hand-label a small portion of the initial try-on images in the training set at the patch level, using bounding boxes for poorly generated regions.

Weakly-Supervised Training. Let x_0, x_1^u, x_1^l be the real human image, the unlabeled initial image, and the labeled initial image with bounding boxes annotating artifacts. Our WSC loss terms are defined as:

$$\begin{aligned} \mathcal{L}_{img} &= -\log(\text{WSC}(x_1^u, C)_{\max}) + \log(1 - \text{WSC}(x_0, C)_{\max}) \\ \mathcal{L}_{pat} &= -\log(\text{WSC}(x_1^l, C) \odot B_{box}) \\ &\quad - \log(1 - \text{WSC}(x_1^l, C) \odot (1 - B_{box})) \end{aligned} \quad (1)$$

where \mathcal{L}_{img} is the image-level loss and \mathcal{L}_{pat} is the patch-level loss. In \mathcal{L}_{img} , $\text{WSC}(\cdot)$ is the output error map and

$\text{WSC}(\cdot)_{\max}$ denotes the spatially max-pooled score in the error map. In \mathcal{L}_{pat} , B_{box} is the spatial binary mask for the annotated regions, thereby maximizing and minimizing the scores for regions within and outside of the annotated boxes respectively. Our final loss is: $\mathcal{L}_{\text{WSC}} = \mathcal{L}_{ins} + \mathcal{L}_{pat}$.

The trained WSC will predict an error map M for the initial image x_1 , which is then used to adjust the noise schedule in the following diffusion process.

5.2. Error-Map-Reweighted SB Formulation

To achieve the refinement goal, our diffusion process extends Schrödinger bridges as formulated in I²SB [24], where we incrementally add noise to the initial image x_1 , and then remove the noise to approximate the refined image x_0 . However, without additional information, a naïvely trained I²SB model must implicitly learn what to refine and what to retain. Our formulation aims to explicitly incorporate prior knowledge of localized generation errors via the error map M into the Schrödinger process by using M to locally scale the noise schedule for the Schrödinger process.

Our choice of locally scaling the noise schedule is based on several observations. For correctly generated regions in x_1 we want the model to directly copy pixels over to x_0 . As such, it would be wasteful to train the model to add and remove noise from these regions. On the other hand, erroneous regions in the initial try-on images, specifically the more noticeable ones, include generation errors that share little to no structural similarity to the target. These errors include examples such as deformed limbs, and distorted textures/fabrics, which in many cases may need more noise added to prevent the model from conditioning too strongly on the original pattern.

As such, we construct our refinement model $F_{\text{EARSB}}(x_1, C, M, P; \theta) \rightarrow x_0$, where the Schrödinger is conditioned on the canonical view garment C , the error map M , and the pose representation P . An overview is shown in Fig. 3, where a Weakly-Supervised Classifier (WSC) first locates the errors in the error map M , then M reweights the noise schedule of the I²SB stochastic process and assigns a higher volume of noise to the highlighted low-quality region "rebel" such that the model can focus on refining it.

Error-Map-Reweighted Diffusion Process. Following I²SB [24], our diffusion Schrödinger bridge maps from the initial image x_1 to the ground truth image x_0 . It fits to the following stochastic process:

$$x_t = \mu_t(x_0, x_1) + \sqrt{\Sigma_t} \cdot \epsilon \quad (2)$$

$$\mu_t = \frac{\bar{\sigma}_t^2}{\bar{\sigma}_t^2 + \sigma_t^2} x_0 + \frac{\sigma_t^2}{\bar{\sigma}_t^2 + \sigma_t^2} x_1, \quad \Sigma_t = \frac{\bar{\sigma}_t^2 \sigma_t^2}{\bar{\sigma}_t^2 + \sigma_t^2} \cdot I,$$

where $\sigma_t^2 = \int_0^t \beta_\tau d\tau$, $\bar{\sigma}_t^2 = \int_t^1 \beta_\tau d\tau$ and β_τ is a symmetrical noise schedule. $\epsilon \sim \mathcal{N}(0, I)$ is random Gaussian noise. The above equation stochastically adds noise and then re-

moves it between x_1 and x_0 .

We extend I²SB such that the noise schedule can vary spatially based on the error map M (obtained from WSC in Sec. 5.1). Good regions will be assigned less noise (*i.e.*, smaller variance) in the diffusion process, while poor quality regions will be assigned more:

$$x_t = \mu_t(x_0, x_1) + \sqrt{\Sigma_t} \cdot \epsilon^r, \quad (3)$$

$$\epsilon^r = M \cdot \epsilon, \quad M = \text{WSC}(x_1, C) \quad (4)$$

where μ_t is the same as in Eq. 2 and ϵ^r is the adaptive noise.

Sampling Process. The initial image x_1 is iteratively refined to x_0 via a denoising/sampling process, where a model predicts the noise distribution at each time step. Different from prior soft-attention-based UNets [19, 27, 37, 38], our denoising model uses cloth-flow-learning UNet for more precise garment deformation [15]. It accepts the garment C , the error map M , the pose representation P , and the noisy image x_t as inputs and predicts the error-adapted noise $\epsilon_\theta^r(\cdot; t)$, where $(\cdot; t)$ omits the inputs M, P, x_t, C . See Supp. B for the detailed model architecture. With the predicted noise $\epsilon_\theta^r(\cdot; t)$, we define our sampling process:

$$\hat{x}_0 = x_t - \sqrt{\Sigma_t} \cdot \epsilon_\theta^r(M, P, x_t, C; t) \quad (5)$$

$$x_{t-\Delta t} = \hat{\mu}_{t-\Delta t}(\hat{x}_0, x_t) + M \cdot \sqrt{\hat{\Sigma}_t} \cdot \epsilon \quad (6)$$

$$\hat{\mu}_{t-\Delta t} = \frac{\sigma_{t-\Delta t}^2}{\sigma_t^2} \hat{x}_0 + \frac{\sigma_t^2 - \sigma_{t-\Delta t}^2}{\sigma_t^2} x_t \quad (7)$$

$$\hat{\Sigma}_t = \frac{\sigma_{t-\Delta t}^2 (\sigma_t^2 - \sigma_{t-\Delta t}^2)}{\sigma_t^2} \quad (8)$$

where $\Delta t > 0$ and it is the sampling interval. Starting from $t = 1$, the process iteratively refines the initial human image x_1 based on the error map M . When M is all ones in Eq. 5, our model reverts to the I²SB formulation. When M is all zeros (*i.e.*, no error), x_1 is believed to be perfect x_1 does not need to be refined in the sampling process.

The training objective of our model is the mean squared error between the predicted noise ϵ_θ^r and the reweighted Gaussian noise ϵ^r

$$\mathcal{L}_{\text{EARSB}} = \mathbb{E}_{t \sim U(0,1)} \|\epsilon_\theta^r(M, P, x_t, C; t) - \epsilon^r\|^2 \quad (9)$$

5.2.1. Further Improvements via Classifier Guidance and Expert Denoisers

Different from prior work that uses object category classifier to guide the sampling process [11], our WSC guidance gives a direction toward the real data distribution. [8] shows that we can estimate the guidance score $\nabla_{x_t} \log p(y|x_t)$ using the denoised clean image \hat{x}_0 : $\nabla_{x_t} \log p(y|x_t) \simeq \nabla_{x_t} \log p(y|\hat{x}_0)$, where y is the fake/real label. Since the label for real data is 0 in WSC, the classifier guidance gives us

$$\hat{\mu}_{t-\Delta t} \leftarrow \hat{\mu}_{t-\Delta t} + M \cdot \hat{\Sigma}_t \cdot \nabla_{x_t} \log p(0|\hat{x}_0) \quad (10)$$

where $p(0|\hat{x}_0) = 1 - \text{WSC}(\hat{x}_0, C)$.

Further improvements are made via expert denoisers [2],

	VITON-HD						DressCode-Upper					
	Unpaired			Paired			Unpaired			Paired		
	FID↓	KID↓	FID↓	KID↓	SSIM↑	LPIPS↓	FID↓	KID↓	FID↓	KID↓	SSIM↑	LPIPS↓
GAN-Based												
HR-VTON [21]	10.75	0.28	8.46	0.26	0.901	0.075	15.26	0.39	11.76	0.32	0.947	0.046
SD-VTON [30]	9.05	0.12	6.47	0.09	0.907	0.070	14.73	0.32	10.99	0.24	0.947	0.042
GP-VTON [36]	8.61	0.86	5.53	0.07	0.913	0.064	26.19	1.71	23.66	1.59	0.816	0.262
SD-Based												
LaDI-VTON [27]	8.95	0.12	6.05	0.08	0.902	0.071	14.88	0.39	11.61	0.32	0.939	0.057
CatVTON [7]	8.87	0.08	5.49	0.07	0.915	0.059	11.91	0.21	7.66	0.10	0.950	0.038
CAT-DM [38]	8.55	0.10	5.98	0.07	0.908	0.067	12.91	0.29	8.58	0.16	0.948	0.038
IDM-VTON [6]	8.59	0.11	5.51	0.09	0.902	0.061	11.09	0.16	6.79	0.12	0.956	0.026
TPD [37]	8.23	0.06	4.86	0.04	0.917	0.057					-	
Stable-VTON [19]	8.20	0.07	5.16	0.05	0.917	0.057					-	
EARSB	8.42	0.07	5.25	0.05	0.918	0.059	10.89	0.13	7.15	0.13	0.961	0.028
EARSB +H2G-UH/FH	8.26	0.06	5.14	0.04	0.919	0.058	10.70	0.11	7.05	0.11	0.965	0.026
EARSB(SD)+H2G-UH/FH	8.04	0.06	4.90	0.03	0.925	0.053	10.41	0.09	6.76	0.08	0.968	0.023

Table 1. Results on VITON-HD [21] and DressCode-Upper [26] KID is multiplied by 100. Results of the diffusion methods are reported at 25 sampling steps.

wherein the trained EARSB model is then split into two models, respectively fine-tuned on denoising ranges $t \in [0, 0.5]$ and $t \in [0.5, 1]$. We default to this in all variants of our method in the next section.

6. Experiments

Datasets. We use VITON-HD, DressCode-Upper, and our synthetic H2G-UH and H2G-FH for training. They include 11,647, 13,564, 12,730, 8,939 training images, respectively. For synthetic data augmentation, we combine VITON-HD [21] with our H2G-UH since both of them include mostly upper-body human images. DressCode-Upper is combined with H2G-FH as both consist of full-body human photos. For evaluation, VITON-HD contains 2,032 (human, garment) test pairs and DressCode-Upper has 1,800 test pairs. Experiments are conducted for both paired and unpaired settings. In the paired setting, the input garment image and the garment in the human image are the same item. Conversely, the unpaired setting uses a different garment image. **Metrics.** We use Structural Similarity Index Measure (SSIM) [33], Fréchet Inception Distance (FID) [16], Kernel Inception Distance (KID) [4], and Learned Perceptual Image Patch Similarity (LPIPS) [39] to evaluate image quality. All the compared methods use the same image size 512x512 and padding when computing the above metrics.

6.1. Comparison with Existing Methods

We compare our EARSB with GAN-based methods HR-VTON [21], SD-VTON[30] and GP-VTON[36], as well as Stable Diffusion (SD) [29] based methods including CAT-DM [38], Stable-VTON [19], TPD [37], IDM-VTON [6] and CatVTON [7]. We control the number of sampling

Methods	GP-GAN	EARSB	Stable-VTON	EARSB
Consistency	42%	58%	38%	62%
Fidelity	39%	61%	45%	55%

Table 2. User studies on VITON-HD. Our EARSB is preferred in an average of 59% cases.

steps by fixing it to 25 in Tab. 1 for all the diffusion methods. The results under different sampling steps on VITON-HD are presented in Fig. 4.

In Tab. 1, EARSB is our model using GAN method GP-VTON [36] to generate the initial image and is trained without synthetic data augmentation. EARSB+H2G-UH/FH trains with either H2G-UH or H2G-FH. We add the upper-body synthetic subset H2G-UH for the upper-body-human dataset VITON-HD, and the full-body synthetic H2G-FH when on DressCode-Upper. EARSB(SD)+H2G-UH/FH further uses diffusion model CatVTON [7] to generate the initial image. EARSB and EARSB+H2G-UH/FH improve the GAN baselines while EARSB(SD)+H2G-UH/FH gains over the SD-based methods. Note that while using the diffusion model to generate the initial image gives better performance in EARSB(SD)+H2G-UH/FH, it also introduces higher computational costs. Overall, our refinement model improves the metrics of existing methods on both datasets, with further improvements from incorporating synthetic training pairs.

User Study. Amazon MTurk workers were asked to compare the image quality on two aspects: texture consistency, and image fidelity, comparing our model against GP-GAN and Stable-VTON. We randomly selected 100 pairs from VITON-HD to evaluate on, assigning at least 3 workers per

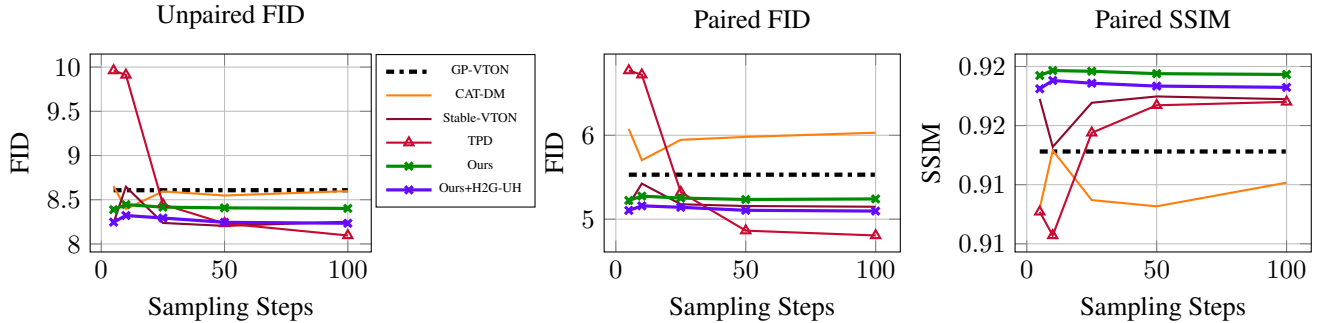


Figure 4. Results on VITON-HD at 5, 10, 25, 50, and 100 sampling steps. Our method consistently improves our baseline starting model GP-VTON (black, dotted line), making it competitive with Stable-VTON (especially at under 50 sampling steps). Legend is shared for all.

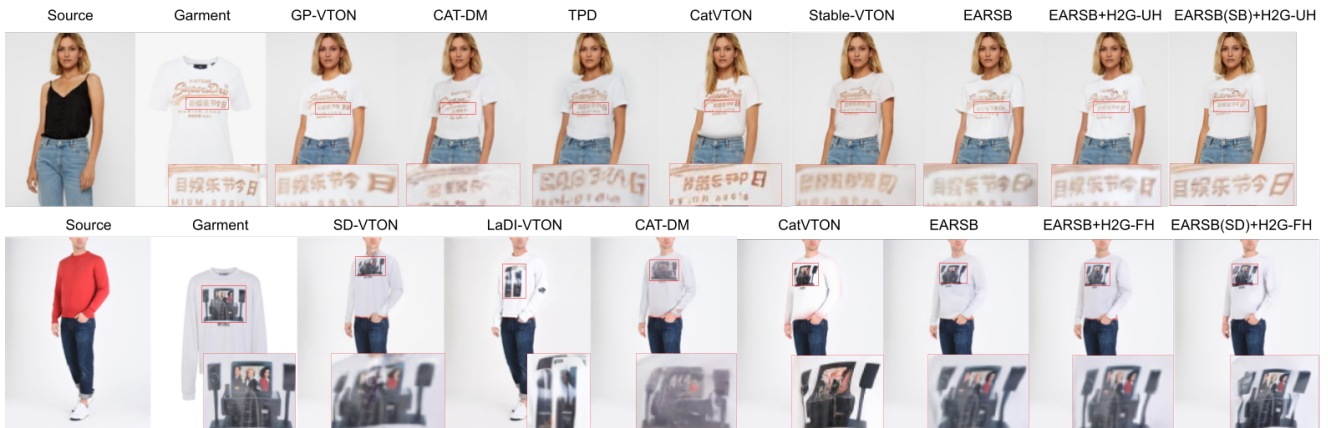


Figure 5. Visualizations on VITON-HD (top row) and DressCode (bottom row). Our EARSB+H2G-UH and EARSB(SD)+H2G-UH better recover the intricate textures in the garment.

image. Tab. 2 reports the study results, where our method is preferred at least 10% more than the GAN-based GP-VTON and the SD-based Stable-VTON (59% overall).

Trade-off Between Sampling Efficiency and Image Quality. Diffusion-generated images often show degraded quality with fewer sampling steps. In EARSB, the spatially adaptive noise schedule can preserve the correct clothing textures in the initial image with a low noise level and only fix the erroneous parts, potentially resulting in less image quality degradation with few steps. In Fig. 4, While other SD-based methods have a sharp performance drop with decreasing sampling steps, EARSB and EARSB +H2G-UH show consistent performance across different sampling steps, demonstrating a better trade-off between image quality and computational efficiency.

Qualitative Results. Fig. 5 gives examples of the generated images using different approaches. The top row is from VITON-HD dataset and the bottom row is from DressCode-Upper. The third images in the two rows are GAN-generated results. We see that our EARSB+H2G-UH/FH in the last column improves the low-quality textures from the GAN-generated images, which are the distorted graphics in the center. More visualized examples can be

found in Supp. F.

6.2. Ablations

Synthetic Pairs Augmentation. Table 3(a) and 3(b) include results of different synthetic data augmentation techniques. In Tab. 3(a), we incorporate H2G-UH into the training of Stable-VTON [19] and CAT-DM [38] on the VITON-HD dataset to validate the effectiveness of synthetic pairs on enhancing existing diffusion methods. Here, we use the number of sampling steps as originally published: 2 for CAT-DM, 50 for Stable-VTON, and 25 for our own EARSB. In Tab. 3(a), +H2G-UH indicates the data augmentation. It shows that training with our synthetic H2G-UH improves most metrics of the above SD-based models.

To determine the importance of the canonical product-view projection, we replace the synthetic garment in each pair with a randomly warped version of the clothing cropped from the real human image, denoted as +W(H2G-UH). The results show that while +W(H2G-UH) hinders the performance of all baseline approaches (*i.e.*, CAT-DM, Stable-VTON and EARSB), incorporating H2G-UH improves most metrics. This demonstrates that the synthetic product-view contributes signifi-

	Unpaired		Paired	
	FID↓	FID↓	SSIM↑	LPIPS↓
(a) CAT-DM [38]	8.56	5.90	0.911	0.067
CAT-DM + W (H2G-UH)	8.73	6.12	0.906	0.071
CAT-DM +H2G-UH	8.36	5.67	0.913	0.063
Stable-VTON [19]	8.25	5.15	0.917	0.056
Stable-VTON + W (H2G-UH)	8.47	5.32	0.910	0.060
Stable-VTON +H2G-UH	8.17	5.04	0.919	0.054
(b) EARSB	8.42	5.25	0.918	0.059
EARSB + W (H2G-UH)	8.68	5.44	0.909	0.063
EARSB + plain H2G-UH	9.64	6.52	0.902	0.073
EARSB pre. H2G-UH	8.35	5.18	0.918	0.059
EARSB +H2G-UH	8.26	5.14	0.919	0.058
(c) Inpaint	9.26	6.33	0.909	0.068
EARSB (w.o. M)	9.21	6.27	0.912	0.061
EARSB (rand(M))	9.13	6.55	0.902	0.071
EARSB (w.o. CG)	8.48	5.32	0.918	0.059

Table 3. Results of ablations on VITON-HD.

cantly to the observed improvements.

Tab. 3(b) explores different ways of incorporating the synthetic data into training. EARSB pre. H2G-UH is pre-trained using the synthetic pairs and finetuned on real data, EARSB+plain H2G-UH is trained using the mixed distribution of the real and synthetic pairs *without* the augmentation label identifying them, and EARSB+H2G-UH uses the mixed data with the identifying label. EARSB pre. H2G-UH is slightly worse than EARSB+H2G-UH. Further, we see the effect of conditioning on the augmentation label, as removing it in EARSB+plain H2G-UH greatly degrades the image quality and causes a significant drop in all metrics.

Error-Aware Noise Schedule. We explore the importance of the error-aware noise schedule in Tab. 3(c). In our error-aware noise schedule, the error map adapts the noise distribution according to the quality of the image patches in the initial image x_1 . This adaptive approach contrasts with a uniform Gaussian noise application across all locations, which would essentially reduce our model to I^2SB . As demonstrated in Tab. 3(c), removing the error map during training (EARSB(w.o. M)) results in a substantial decline across all metrics. In another setting, instead of learning the refinement with adaptive noise distribution, we train an inpainting model Inpaint to directly regenerate the erroneous regions in x_0 using the same model architecture. In this experiment, the image patch in x_0 is defined to be erroneous if its mean confidence in M is greater than 0.5. In Tab. 3(c), the inpainting model Inpaint shows degraded performance, demonstrating the importance of learning the error-to-ground-truth refinement in our model. Furthermore, we explored using a random error map during the sampling process (EARSB(rand(M))), which also leads to diminished performance. These results underscore the im-

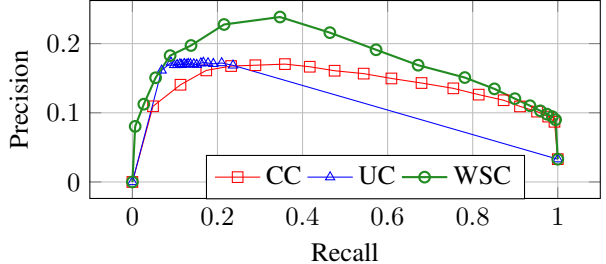


Figure 6. The precision-recall curve for retrieving annotated errors at the pixel level, comparing our WSC to two fully unsupervised baselines (UC, CC). WSC performs best at retrieving generation artifacts at a nominal labeling cost.

portance of a meaningful error map in precisely locating and enhancing targeted regions. Additionally, the slight performance degradation observed when removing the classifier guidance (EARSB(w.o. CG)) suggests that the error map employed in our classifier guidance also contributes to overall image quality improvement. Collectively, these findings highlight the crucial role of our adaptive noise schedule in achieving superior results.

Weakly-Supervised Classifier. Our weakly supervised classifier highlights low-quality regions in the initial image x_1 with only a few hours of labeling. To validate its effectiveness, we train two ablations of our WSC: the Unsupervised Classifier (UC) that only uses image labels (*i.e.*, fake or real), and the Fake/Real Composite Classifier (CC). CC uses both image fake/real labels as well as fake region-level labels which are created by compositing real image patches and fake image patches. The compositing is a fully automatic alternative to manual labeling that provides patch-level labels. We annotated 100 images in the test set to validate their effectiveness. Fig. 6 shows the pixel-level precision-recall curve for retrieving annotated artifact pixels within the bounding boxes using the classifiers’ confidence maps. It is clear that weak supervision remains an incredibly cost-effective approach.

7. Conclusions

This paper proposed an approach that addresses two shortcomings of prior work on virtual try-on. First, we address the limited data availability by introducing a human-to-garment model that generates (human, synthetic garment) pairs from a single image of a clothed individual. Second, we propose a refinement model EARSB that surgically targets localized generation errors from the output of a prior model. EARSB improves the low-quality region of an initially generated image based on a spatially-varying noise schedule that targets known artifacts. Experiments on two benchmark datasets demonstrate that our synthetic data augmentation improves the performance of existing methods and that EARSB enhances the quality of the images generated by prior models.

References

- [1] Sina Alemohammad, Ahmed Imtiaz Humayun, Shruti Agarwal, John Collomosse, and Richard Baraniuk. Self-improving diffusion models with synthetic data. *arXiv preprint arXiv:2408.16333*, 2024. 2
- [2] Yogesh Balaji, Seungjun Nah, Xun Huang, Arash Vahdat, Jiaming Song, Qinsheng Zhang, Karsten Kreis, Miika Aittala, Timo Aila, Samuli Laine, Bryan Catanzaro, Tero Karras, and Ming-Yu Liu. ediff-i: Text-to-image diffusion models with ensemble of expert denoisers. *arXiv preprint arXiv:2211.01324*, 2022. 5, 11
- [3] Alberto Baldrati, Davide Morelli, Giuseppe Cartella, Marcella Cornia, Marco Bertini, and Rita Cucchiara. Multimodal garment designer: Human-centric latent diffusion models for fashion image editing. In *CVPR*, 2023. 2
- [4] Mikołaj Bińkowski, Danica J Sutherland, Michael Arbel, and Arthur Gretton. Demystifying MMD GANs. In *ICLR*, 2018. 6
- [5] Tim Brooks, Aleksander Holynski, and Alexei A Efros. Instructpix2pix: Learning to follow image editing instructions. In *CVPR*, 2023. 2
- [6] Yisol Choi, Sangkyung Kwak, Kyungmin Lee, Hyungwon Choi, and Jinwoo Shin. Improving diffusion models for virtual try-on. In *ECCV*, 2024. 6
- [7] Zheng Chong, Xiao Dong, Haoxiang Li, Shiyue Zhang, Wenqing Zhang, Xujie Zhang, Hanqing Zhao, and Xiaodan Liang. Catvton: Concatenation is all you need for virtual try-on with diffusion models. *arXiv preprint arXiv:2407.15886*, 2024. 2, 6
- [8] Hyungjin Chung, Jeongsol Kim, Michael T Mccann, Marc L Klasky, and Jong Chul Ye. Diffusion posterior sampling for general noisy inverse problems. In *ICLR*, 2023. 5
- [9] Aiyu Cui, Sen He, Tao Xiang, and Antoine Toisoul. Learning garment densepose for robust warping in virtual try-on. *arXiv preprint arXiv:2303.17688*, 2023. 13
- [10] Damien Dablain, Bartosz Krawczyk, and Nitesh V Chawla. Deepsmote: Fusing deep learning and smote for imbalanced data. *IEEE Transactions on Neural Networks and Learning Systems*, 34(9):6390–6404, 2022. 2
- [11] Prafulla Dhariwal and Alexander Nichol. Diffusion models beat gans on image synthesis. *NeurIPS*, 2021. 2, 5
- [12] Jianglin Fu, Shikai Li, Yuming Jiang, Kwan-Yee Lin, Chen Qian, Chen Change Loy, Wayne Wu, and Ziwei Liu. Stylegan-human: A data-centric odyssey of human generation. In *European Conference on Computer Vision*, 2022. 2, 3
- [13] Sicheng Gao, Xuhui Liu, Bohan Zeng, Sheng Xu, Yanjing Li, Xiaoyan Luo, Jianzhuang Liu, Xiantong Zhen, and Baochang Zhang. Implicit diffusion models for continuous super-resolution. In *CVPR*, 2023. 2
- [14] Rıza Alp Güler, Natalia Neverova, and Iasonas Kokkinos. Densepose: Dense human pose estimation in the wild. In *CVPR*, 2018. 3
- [15] Xintong Han, Xiaojun Hu, Weilin Huang, and Matthew R Scott. Clothflow: A flow-based model for clothed person generation. In *CVPR*, 2019. 2, 3, 5, 11
- [16] Martin Heusel, Hubert Ramsauer, Thomas Unterthiner, Bernhard Nessler, and Sepp Hochreiter. GANs trained by a two time-scale update rule converge to a local nash equilibrium. In *NeurIPS*, 2017. 6
- [17] Heewoo Jun, Rewon Child, Mark Chen, John Schulman, Aditya Ramesh, Alec Radford, and Ilya Sutskever. Distribution augmentation for generative modeling. In *ICML*, 2020. 3
- [18] Tero Karras, Miika Aittala, Janne Hellsten, Samuli Laine, Jaakko Lehtinen, and Timo Aila. Training generative adversarial networks with limited data. *NeurIPS*, 2020. 2
- [19] Jeongho Kim, Guojung Gu, Minh Park, Sunghyun Park, and Jaegul Choo. Stableviton: Learning semantic correspondence with latent diffusion model for virtual try-on. In *CVPR*, 2024. 1, 2, 5, 6, 7, 8
- [20] Ananya Kumar, Aditi Raghunathan, Robbie Matthew Jones, Tengyu Ma, and Percy Liang. Fine-tuning can distort pre-trained features and underperform out-of-distribution. In *ICLR*, 2022. 3
- [21] Sangyun Lee, Gyojung Gu, Sunghyun Park, Seunghwan Choi, and Jaegul Choo. High-resolution virtual try-on with misalignment and occlusion-handled conditions. In *ECCV*, 2022. 2, 3, 6, 11, 12
- [22] Nannan Li, Qing Liu, Krishna Kumar Singh, Yilin Wang, Jianming Zhang, Bryan A Plummer, and Zhe Lin. Unihuman: A unified model for editing human images in the wild. In *CVPR*, 2024. 2, 3
- [23] Zhi Li, Pengfei Wei, Xiang Yin, Zejun Ma, and Alex C Kot. Virtual try-on with pose-garment keypoints guided inpainting. In *ICCV*, 2023. 1, 2
- [24] Guan-Hong Liu, Arash Vahdat, De-An Huang, Evangelos A Theodorou, Weili Nie, and Anima Anandkumar. I2sb: image-to-image schrödinger bridge. In *ICML*, 2023. 2, 3, 4, 5
- [25] Ziwei Liu, Ping Luo, Shi Qiu, Xiaogang Wang, and Xiaoou Tang. Deepfashion: Powering robust clothes recognition and retrieval with rich annotations. In *CVPR*, 2016. 2, 3
- [26] Davide Morelli, Matteo Fincato, Marcella Cornia, Federico Landi, Fabio Cesari, and Rita Cucchiara. Dress code: High-resolution multi-category virtual try-on. In *CVPR*, 2022. 2, 6
- [27] Davide Morelli, Alberto Baldrati, Giuseppe Cartella, Marcella Cornia, Marco Bertini, and Rita Cucchiara. LaDIVTON: Latent Diffusion Textual-Inversion Enhanced Virtual Try-On. In *ACM Multimedia*, 2023. 5, 6
- [28] Shuliang Ning, Duomin Wang, Yipeng Qin, Zirong Jin, Baoyuan Wang, and Xiaoguang Han. Picture: Photorealistic virtual try-on from unconstrained designs. In *CVPR*, 2024. 2
- [29] Robin Rombach, Andreas Blattmann, Dominik Lorenz, Patrick Esser, and Björn Ommer. High-resolution image synthesis with latent diffusion models. In *CVPR*, 2022. 6, 11
- [30] Sang-Heon Shim, Jiwoo Chung, and Jae-Pil Heo. Towards squeezing-averse virtual try-on via sequential deformation. In *AAAI*, 2024. 1, 2, 3, 6, 11, 12
- [31] C Shivashankar and Shane Miller. Semantic data augmentation with generative models. In *CVPR*, 2023. 2

- [32] Yang Song and Stefano Ermon. Generative modeling by estimating gradients of the data distribution. *NeurIPS*, 2019. [2](#)
- [33] Zhou Wang, Alan C Bovik, Hamid R Sheikh, and Eero P Simoncelli. Image quality assessment: from error visibility to structural similarity. *IEEE Transactions on Image Processing*, 13(4):600–612, 2004. [6](#)
- [34] Navve Wasserman, Noam Rotstein, Roy Ganz, and Ron Kimmel. Paint by inpaint: Learning to add image objects by removing them first. *arXiv preprint arXiv:2404.18212*, 2024. [2](#)
- [35] Zhenyu Xie, Zaiyu Huang, Fuwei Zhao, Haoye Dong, Michael Kampffmeyer, and Xiaodan Liang. Towards scalable unpaired virtual try-on via patch-routed spatially-adaptive gan. *NeurIPS*, 2021. [2](#), [3](#)
- [36] Zhenyu Xie, Zaiyu Huang, Xin Dong, Fuwei Zhao, Haoye Dong, Xijin Zhang, Feida Zhu, and Xiaodan Liang. GP-VTON: Towards general purpose virtual try-on via collaborative local-flow global-parsing learning. In *CVPR*, 2023. [1](#), [2](#), [6](#), [11](#), [12](#)
- [37] Xu Yang, Changxing Ding, Zhibin Hong, Junhao Huang, Jin Tao, and Xiangmin Xu. Texture-preserving diffusion models for high-fidelity virtual try-on. In *CVPR*, 2024. [1](#), [2](#), [5](#), [6](#)
- [38] Jianhao Zeng, Dan Song, Weizhi Nie, Hongshuo Tian, Tongtong Wang, and An-An Liu. Cat-dm: Controllable accelerated virtual try-on with diffusion model. In *CVPR*, 2024. [3](#), [5](#), [6](#), [7](#), [8](#), [12](#)
- [39] Richard Zhang, Phillip Isola, Alexei A Efros, Eli Shechtman, and Oliver Wang. The unreasonable effectiveness of deep features as a perceptual metric. In *CVPR*, 2018. [6](#)
- [40] Luyang Zhu, Dawei Yang, Tyler Zhu, Fitsum Reda, William Chan, Chitwan Saharia, Mohammad Norouzi, and Ira Kemelmacher-Shlizerman. TryOnDiffusion: A tale of two unets. In *CVPR*, 2023. [1](#)

APPENDIX

A. Implementations Details

For generating the initial image x_1 in our EARSB training, we employ three try-on GAN models: HR-VTON [21] and SD-VTON [30] and GP-VTON [36]. All human images are processed to maintain their aspect ratio, with the longer side resized to 512 pixels and the shorter side padded with white pixels to reach 512. During training, images undergo random shifting and flipping with a 0.2 probability. The weakly-supervised classifier is trained for 100K iterations with a batch size of 8, while the human-to-garment GAN is trained for 90K iterations with a batch size of 16. EARSB+H2G-UH/FH is trained for 300K iterations with a batch size of 32, incorporating 15% synthetic pairs in each batch. The first 200K iterations are trained on $t \in [0, 1]$ while the following 100k iterations are finetuned on $t \in [0, 0.5]$ and $t \in [0.5, 1]$ respectively following [2]. All models utilize the AdamW optimizer with a learning rate of 10^{-4} .

For inference, we select the GAN model that demonstrates better performance on each dataset to generate the initial image. Specifically, we employ GP-VTON [36] for VITON-HD and SD-VTON [30] for DressCode-Upper. During the sampling process, the guidance score in Eq. (10) is scaled by a factor of 6 and clamped to the range $[-0.3, 0.3]$.

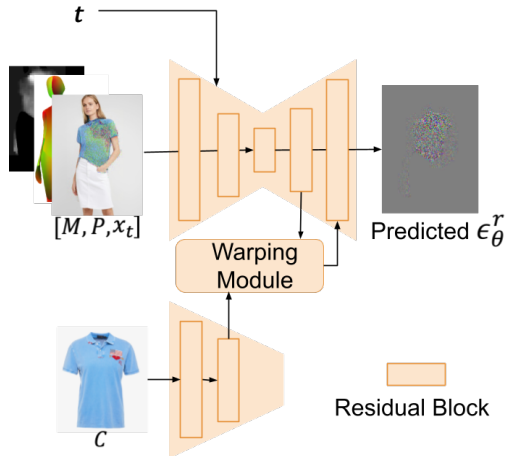


Figure 7. Architecture of our UNet in EARSB.

B. UNet Architecture

EARSB UNet. The UNet architecture in EARSB consists of residual blocks and garment warping modules. It processes the concatenation of the error map M , pose representation P , and noisy image x_t to predict the noise distribution ϵ_θ^r at time t . The UNet encoder has 21 residual blocks,

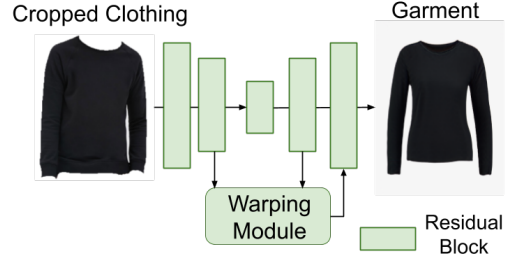


Figure 8. Architecture of our UNet in the human-to-garment model.

with the number of channels doubling every three blocks to a maximum of 256. Similarly, the garment encoder has 21 residual blocks but reaches a maximum of 128 channels. The decoder mirrors the encoder’s structure, with extra garment warping modules. As shown in Fig. 7, each of the first 15 residual blocks in the UNet decoder is followed by a convolutional warping module. These modules concatenate encoded garment features and UNet-decoded features to predict a flow-like map for spatially warping the encoded garment features. The warped features are then injected into the subsequent decoder layer via input concatenation. Following [29], all residual blocks and flow-learning modules incorporate timestep embeddings to renormalize latent features.

Human-to-Garment UNet. Our human-to-garment UNet architecture is adapted from the model proposed in [15]. As illustrated in Fig. 8, it shares similarities with the UNet in EARSB, but with two key distinctions: a) It is not timestep-dependent and takes cropped clothing as input to generate its product-view image. b) The garment warping module utilizes the i_{th} clothing features from both the encoder and decoder to learn a flow-like map, rather than using encoded features from the human.

C. Visualizing Error Maps

Our EARSB focuses on fixing specific errors and therefore can save the sampling cost when initial predictions are sufficiently good. For example, in the first row of Fig. 9, the error map highlights the graphics and text in the initial image. This low-quality part is being refined progressively as the number of sampling steps increases from 5 to 100. At the same time, other parts that our weakly-supervised classifier believes to be sufficiently good, which are mostly the solid-color areas, are kept well regardless of the number of sampling steps. Therefore, for an initial image whose error map has almost zero values, we can choose to use fewer steps in sampling. On the contrary, for an initial image whose error map has high confidence, we should assign more sampling steps to it to improve the image quality.



Figure 9. Results on different time steps. Our error map focuses on low-quality regions and maintains the quality of the sufficiently good regions.

	HR-VTON [21]	SD-VTON [30]	GP-VTON [36]
Baseline	10.75	9.05	8.61
CAT-DM [38]	10.03	8.76	8.55
EARSB	9.11	8.69	8.42

Table 4. FID scores of using different try-on GAN models to generate the initial image under the unpaired setting.

D. Ablations on the Quality of the Initial Image

In Tab. 4 we include the FID results of using different try-on GAN models to generate the initial image under the unpaired setting. Baseline means the GAN baseline. As previously stated in Sec. 4.1., we can draw three conclusions from the results: a) our EARSB can refine the GAN-generated image over the GAN baseline; b) the quality of the initial image x_1 is positively correlated with the quality of the sampled \hat{x}_0 ; c) our model achieves higher gains over CAT-DM, which also tries to refine the GAN-generated im-

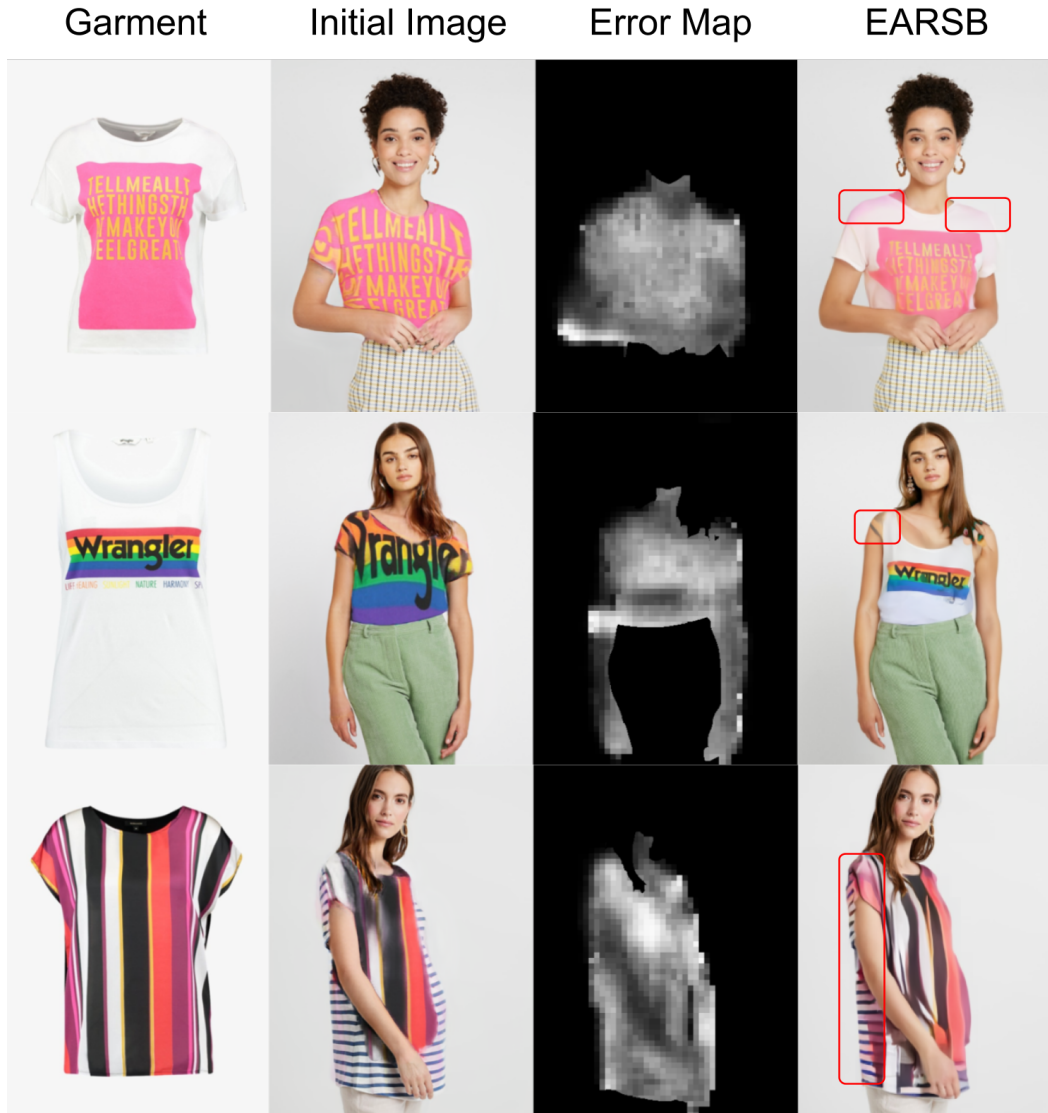


Figure 10. Failure cases on VITON-HD where the initial image has a poor-quality.

age but without error-aware noise schedule.

E. Limitations

While our human-to-garment model can effectively generate synthetic paired data for try-on training augmentation, it has some imperfections. The overall quality of synthetic garments is regulated by our filtering criteria (Sec. 3.1.2), yet minor texture deformations occasionally occur. For instance, in Fig. 11, the second pair of the first row shows a misaligned shirt placket in the synthetic garment. This limitation stems partly from the fact that our model is trained in the image domain which lacks 3D information. A potential solution is to utilize DensePose representations extracted from the garment as in [9].

A key constraint of our EARSB is its refinement-based nature, which makes the generated image dependent on the initial image. We assume that the initial image from a try-on GAN model is of reasonable quality, requiring only partial refinement. Consequently, if the initial image is of very poor quality, our refinement process cannot completely erase and regenerate an entirely new, unrelated image. Fig. 10 illustrates this limitation: in the first row, the initial image severely mismatches the white shirt with pink graphics. With EARSB refinement, while the shirt is correctly re-wrapped, color residuals from the initial image persist around the shoulder area.

	FID	KID	SSIM	LPIPS
VITON-HD	14.81	0.42	0.849	0.229
DressCode-Upper	18.92	0.59	0.832	0.257

Table 5. Human-to-Garment results under 1024x1024 image resolution.

F. Additional Visualizations

Figures 11 and 12 showcase exemplars from our synthesized datasets H2G-UH and H2G-FH, respectively. We also report quantitative results in Table 5 to evaluate our human-to-garment model on VITON-HD and DressCode-Upper. The generated garment images in Figures 11 and 12 closely mimic the product view of the clothing items, accurately capturing both the shape and texture of the original garments worn by the individuals. This approach to creating synthetic training data for the virtual try-on task is both cost-effective and data-efficient, highlighting the benefits of our proposed human-to-garment model.

Figures 13 and 14 give visualized results of the proposed EARSB and EARSB+H2G-UH. In contrast to previous approaches, EARSB specifically targets and enhances low-quality regions in GAN-generated images, which typically correspond to texture-rich areas. This targeted improvement is evident in the last row of Fig. 13, where EARSB more accurately reconstructs text *freinds*, and in the third row, where it successfully generates four side buttons. Furthermore, the incorporation of our synthetic dataset H2G-UH with EARSB leads to even more refined details in the generated images, demonstrating the synergistic effect of our combined approach.

G. Ethics

Our work on virtual try-on technology can improve user shopping experiences and reduce clothing returns, which could have positive environmental impacts by reducing waste and transportation emissions. However, we acknowledge several potential ethical considerations:

- **Bias and representation:** We strive for diversity in our training data to ensure the model performs equitably across different body types, skin tones, and ethnicities. However, biases may still exist, and further work is needed to assess and mitigate these.
- **Misuse potential:** While intended for benign purposes, this technology could potentially be misused to create misleading or non-consensual images. We strongly condemn such uses and will explore safeguards against misuse in future work.
- **Environmental impact:** While our method aims to reduce environmental impact from returns, the computational resources required for training and running these models

have their own carbon footprint. We are committed to optimizing our models for efficiency. We believe the potential benefits of this technology outweigh the risks, but we remain vigilant about these ethical considerations and are committed to addressing them as our research progresses.



Figure 11. Visualized examples of the (human, synthetic garment) pairs on our proposed H2G-UH.

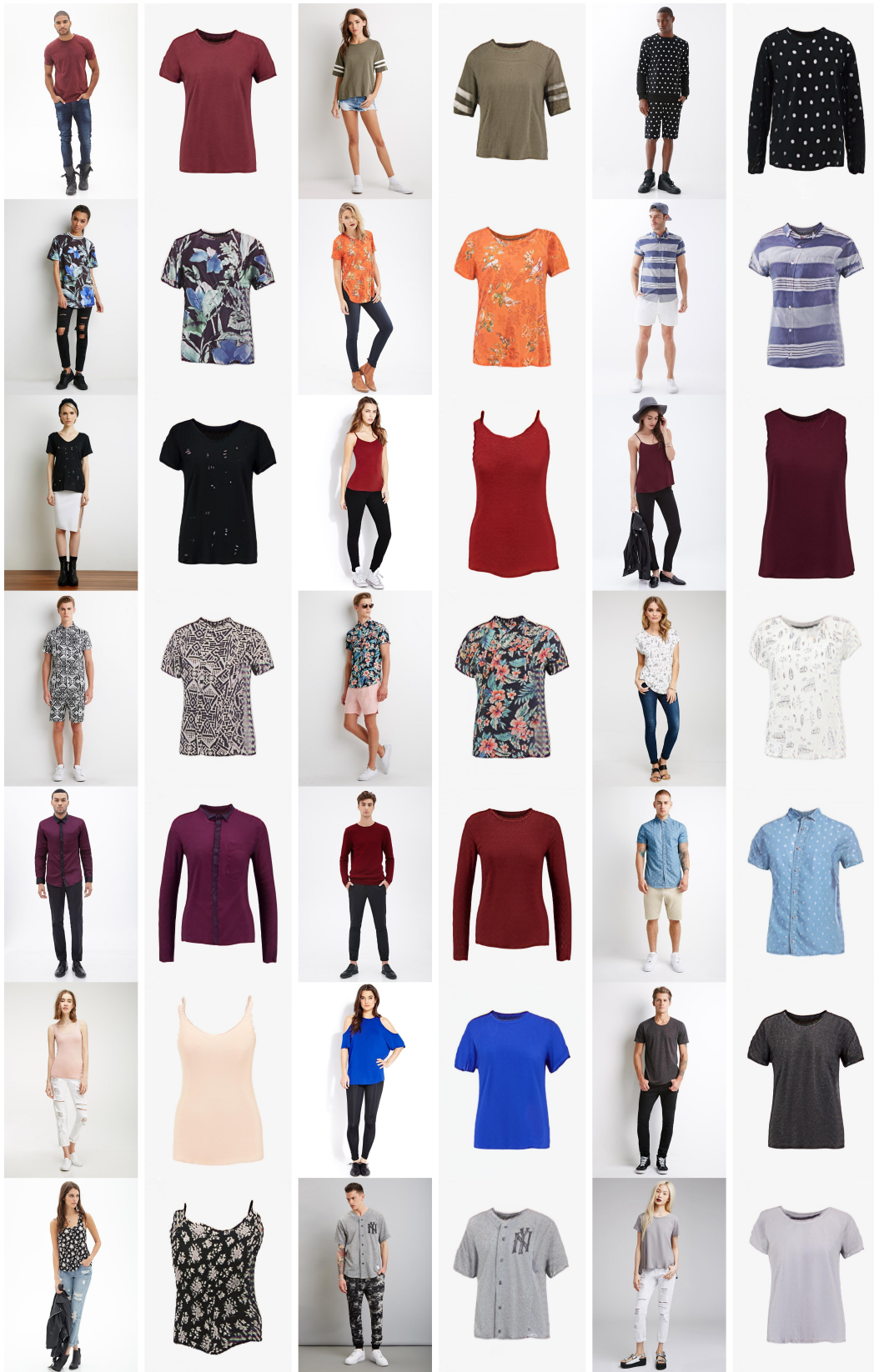


Figure 12. Visualized examples of the (human, synthetic garment) pairs on our proposed H2G-FH.

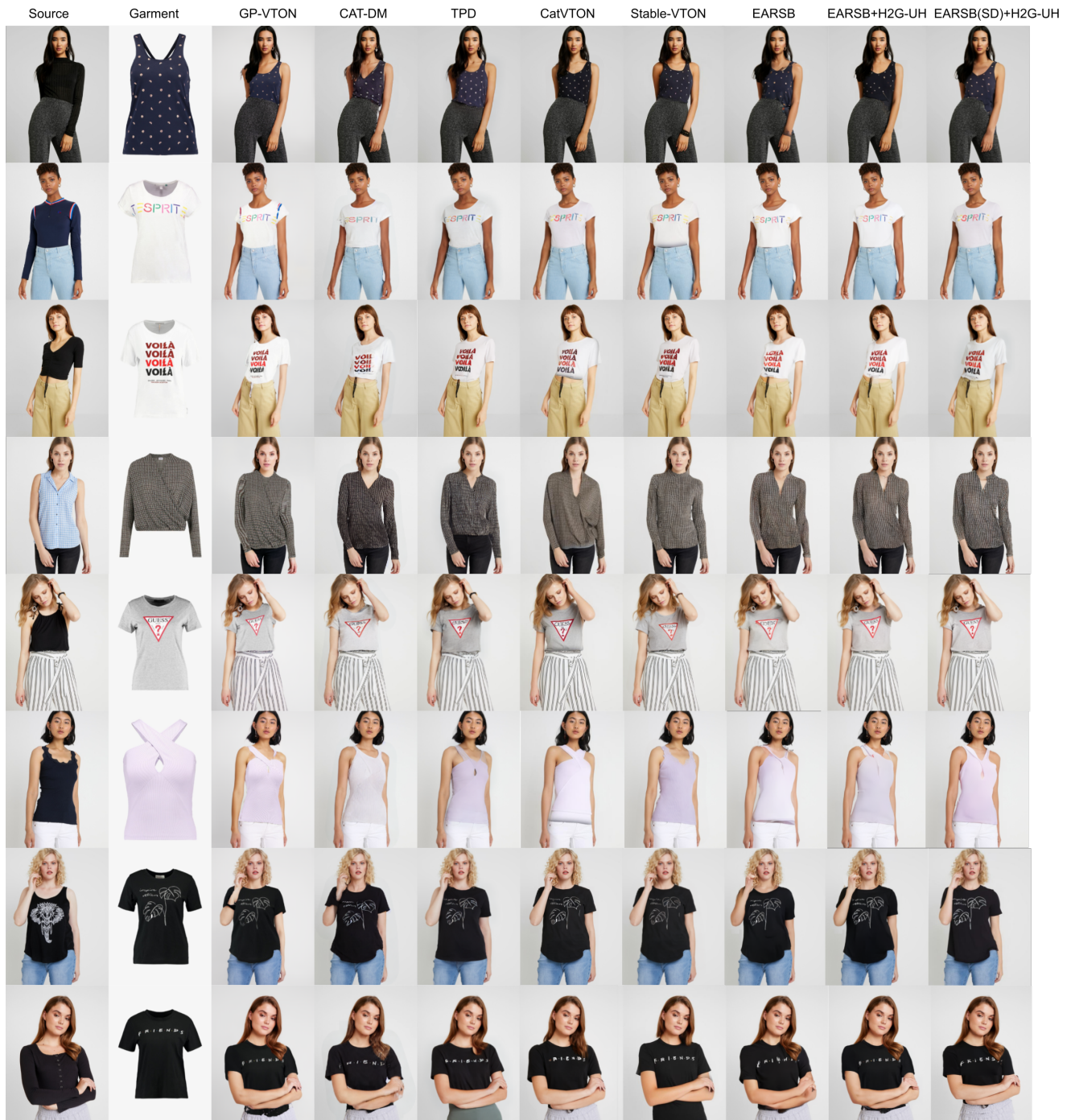


Figure 13. Visualized examples on VITON-HD. Our EARSB and EARSB+H2G-UH better recovers the intricate textures in the garment.

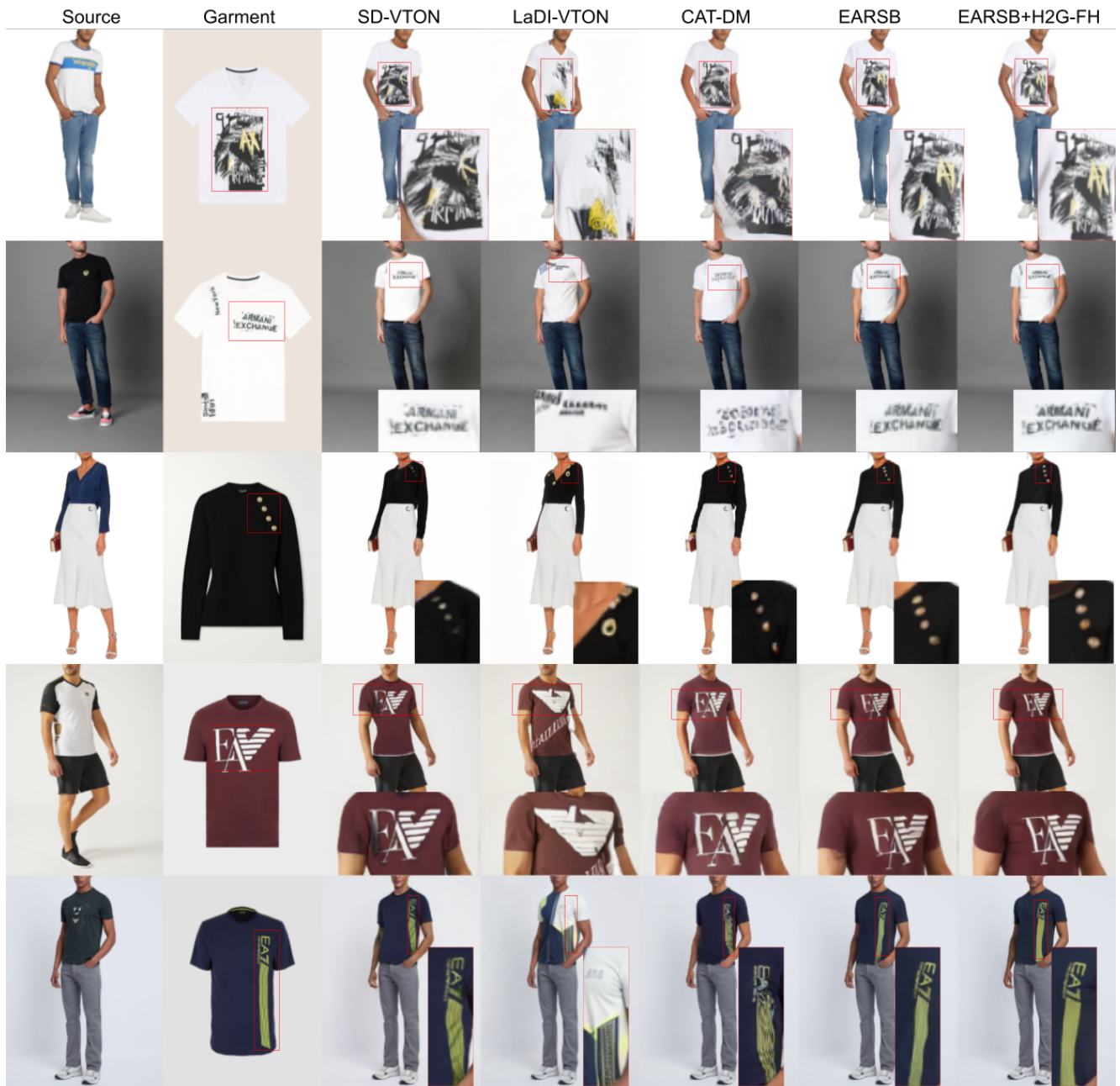


Figure 14. Visualized examples on DressCode-Upper. Our EARSB and EARSB+H2G-UH better reconstructs the texts and graphics in the garment.